Supplementary Information for

Water Transport in Periodic Mesoporous Organosilica Materials

Benedikt J. Mietner

Institute of Inorganic and Applied Chemistry, University of Hamburg, Hamburg, Germany

The Hamburg Centre for Ultrafast Imaging, Hamburg, Germany

Michael Fröba

Institute of Inorganic and Applied Chemistry, University of Hamburg, Hamburg, Germany

The Hamburg Centre for Ultrafast Imaging, Hamburg, Germany

Email: froeba@chemie.uni-hamburg.de

Phone: +49 4042838 3100

Rustem Valiullin

Felix Bloch Institute for Solid State Physics, University of Leipzig, Leipzig, Germany

Email: valiullin@uni-leipzig.de

Phone: +49 341 9732515

1. Synthesis of the materials

MCM-41 silica powder was prepared following the procedure similar to a previously described method.[1] Tetramethylammonium hydroxide (TMAOH, 0.60 mmol, 25 % in water, ABCR) and sodium hydroxide (NaOH, 1.1 mmol, Merck) were dissolved in 4 mL deionized water. SiO_2 (8.1 mmol, fumed Silica, Aldrich) were added under vigorous stirring and the mixture was kept at 40 °C overnight. Then, alkyltrimethylammonium bromide surfactant in deionized water (4 mL) was added and stirred at room temperature for 20 hours. Afterwards, the solution was transferred into a Teflon-lined steel autoclave and statically heated to 140 °C for 24 h. The resultant white precipitate was collected by filtration and washed with 200 mL deionized water. After drying at 60 °C, the white powder was calcined in air at 550 °C for 4 hours (heating rate: 1 $K \cdot min^{-1}$). PMO precursors of 1,4-Bis(triethoxysilyl)benzene (BTEB), 4,4′-Bis(triethoxysilyl)-1,1′-biphenyl (BTEBP) and 2,5-[(E)-2-bis(triethoxy- silyl)vinyl]aniline (BTEVA) were prepared as previously described[2,3]. PMO powder was prepared according to the following procedure. NaOH and the alkyltrimethylammonium bromide surfactant were dissolved in deionized water. The precursor was added at room temperature and the mixtures were stirred for 20 hours. The mixtures were transferred into a Teflon-lined steel autoclave and statically heated to 95 °C or 100 °C for 24 h. The resultant precipitate was collected by filtration and washed with 200 mL deionized water. After drying at 60 °C, the powder was extracted with a mixture of ethanol and hydrochloric acid (EtOH:HCl (37 %), 97:3, v/v) using a Soxhlet extractor. The exact compositions used for the synthesis of MCM-41 silica and the PMOs are summarized in Table 1. The porosity and the pore structure of the dried materials were characterized by powder X-ray diffraction and nitrogen adsorption as described in the supplementary Information.

Table S1: Compositions of the synthesis mixtures leading to MCM-41 silica and the PMOs

Precursor type	Precursor amount	Water [mL]	NaOH [mmol]	TMAOH [mmol]	Surfactant type	Surfactant amount [ ]	Hydroth. temp. [°C]	Label
MCM-41								
Silica	0.485 g	8	1.1	0.60	C_{12}TAB	0.739	140	MCM-41
B-PMO								
BTEB	0.44 mL	40	6.8	-	C_{14}TAB	0.08	95	B-PMO
BP-PMO								
BTEBP	0.63 mL	50	25	-	C_{18}TAB	0.63	95	BP-PMO
A-PMO								
BTEVA	0.40 g	10	0.16	-	C_{14}TAB	0.35	90	A-PMO

2. XRD analysis of the porous materials

Powder X-ray diffraction patterns were recorded at room temperature with a STOE Stadi P diffractometer in a transmission mode using filtered Cu Kα radiation (40 kV, 45 mA; counting time: 2 s; steps: 0.01° (2θ)).

All the synthesized materials were characterized by powder XRD to get information about the pore arrangement and the crystal-like pore wall structure. In Figure S1a, the XRD patterns of the MCM-41 materials show three to five reflections in the small angle region ($2\theta < 10°$), indicating that the materials exhibit hexagonally ordered pore structures. In Figure S1b, additional reflections at the equal distant in the medium angle area ($10° < 2\theta < 30°$) of the reflection pattern are observed for the benzene-, biphenyl- and aniline-PMOs, suggesting that these PMO materials possess a crystal-like pore wall structuring as well as periodic arrangement of the pores in mesoscale.[3–5]

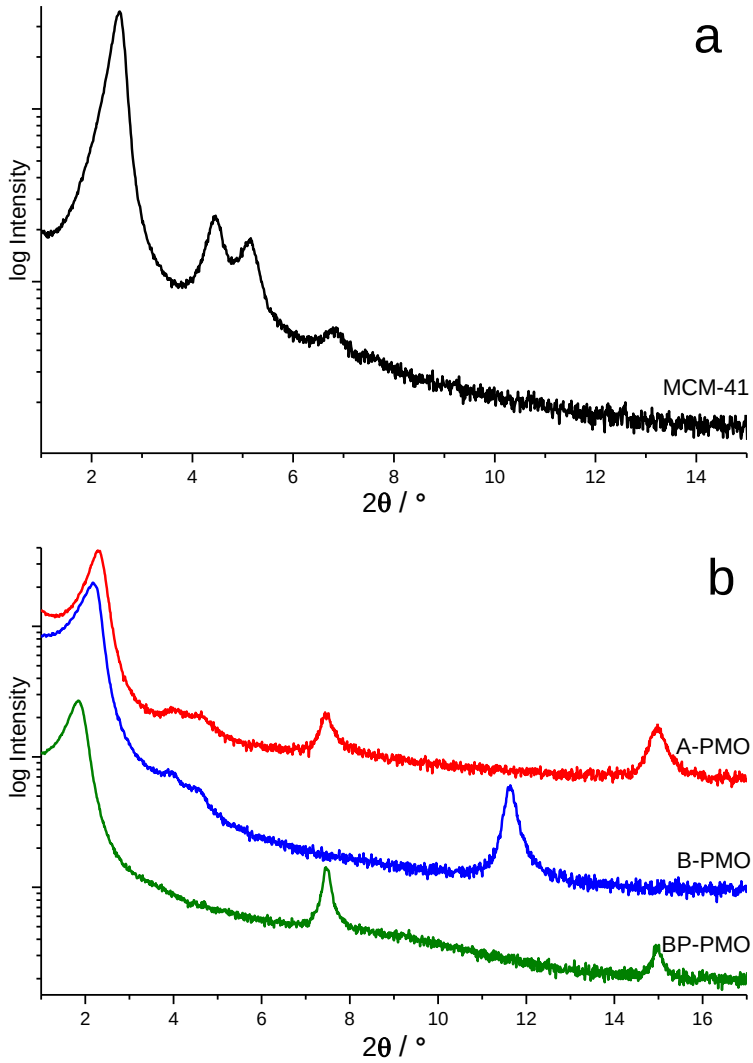

Figure S1. XRD patterns of the MCM-41 materials and the benzene-, biphenyl- and aniline-PMOs with crystal-like pore wall structuring.

3. Nitrogen adsorption analysis

Nitrogen physisorption data were recorded at 77.3 K with a Quantachrome QuadraSorb or Autosorb-6-MP using 99.9990 % purity N_2. The samples were previously degassed with a Quantachrome MasterPrep Degasser-Station at 333 K for 20 h at a maximum pressure of 0.01 mbar. The analysis was carried out with the ASiQwin 2.01 software from Quantachrome. The BET surface areas were calculated from the linear section at p/p_0 = 0.03-0.3 in the

adsorption branch while the NLDFT pore size distributions were calculated from the adsorption branch at p/p0 = 0.0002 - 1 using the NLDFT- N_2- silica adsorption branch kernel at 77 K based on a cylindrical pore model.

To analyze the porosity of the materials, N_2 physisorption measurements were carried out. In Figure S2, the results of the N_2-pysisorption measurements are shown. In Figure S2a the isotherms are normalized for better comparison of the capillary condensation step. It can be easily seen that pore condensation step in every material occurs at the same relative pressure. This indicates a similar pore size of the different materials. As shown in Figure S2b the NLDFT pore size distributions of the materials yield a narrow half width and a matching pore size. The results of the N_2 physisorption measurements and a geometrical calculated density of the solid phase of the materials are summarized in Table S2.

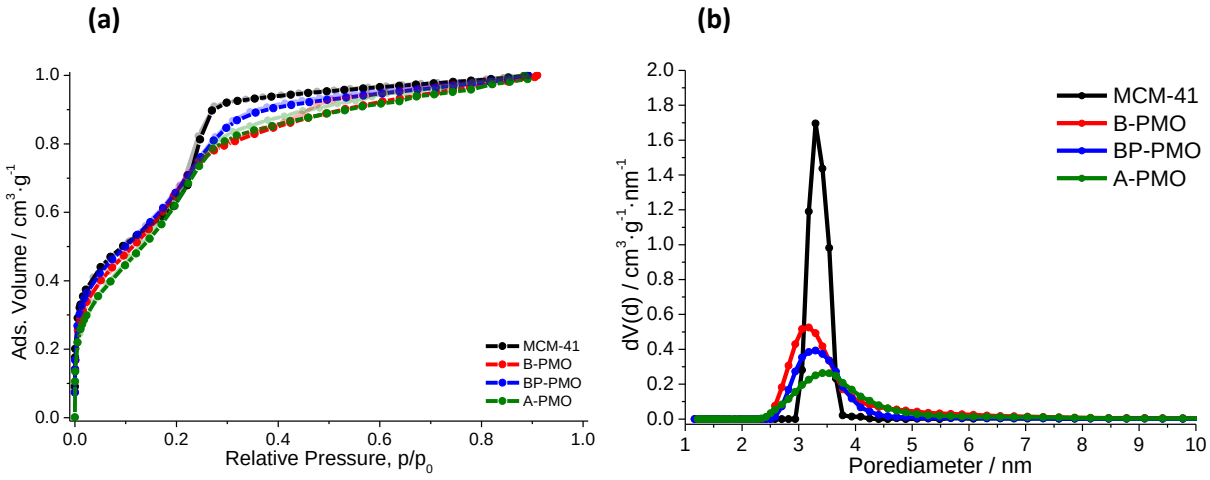

Figure S2. (a) Normalized N_2 physisorption isotherms of the materials (b) Pore size distributions of the materials deduced from the N_2 physisorption adsorption.

Table S2. Specific surface areas, pore sizes, pore volumes and solid densities of the various MCM-41 and PMOs.

Label	SSA [m^2g^{-1}]	Pore Size [nm]	Pore Volume [cm^3g^{-1}]	Density of solid (calc.) [gcm^{-3}]
MCM-41	1151	3.3	0.810	2.03
A-PMO	922	3.3	0.607	1.68
B-PMO	1354	3.2	0.63	1.66
BP-PMO	877	3.3	0.430	1.12

4. Surface properties

Surface polarity and hydrophobicity, as determined by the organic bridging group, can be deduced from water adsorption shown in Figure S3. In comparison to MCM-41 silica yielding pore condensation at p/p_0 = 0.49, the pore condensation step is shifted significantly to higher relative pressure for BP-PMO (p/p_0 = 0.58) and B-PMO (p/p_0 = 0.50) and to lower pressure for A-PMO (p/p_0 = 0.44). Minor difference in the onset pressure of the pore condensation step between MCM-41 and B-PMO is presumably associated with the broader pore size distribution in the B-PMO sample. The amounts of adsorbed water measured at p/p_0 = 0.2 are 0.28 and 0.98 mmol/g for BP- and B-PMO, respectively. These low levels of water uptake suggest that BP-PMO provides the highest hydrophobicity, followed by B-PMO. A-PMO and MCM-41 silica adsorb 1.55 and 2.59 mmol/g of water, respectively, indicating that these materials are more hydrophilic than BP- and B-PMO. Nevertheless, hydrophobicity cannot be quantified straightforward from the amounts of water uptake since the density of materials needs to be considered.

When the densities of the solid phases of the two materials are taken into account one end up with volume-specific adsorption amounts: MCM-41 silica and A-PMO adsorb 0.76 and 1.54 mmol/cm^3 water. This means that the A-PMO material is more hydrophilic than the MCM-41. But the densitys of the solid phases of the materials are calculated using a geometrical approach

with data from XRD and the pore sizes and pore volumes from N_2 physisorption experiments. This means they are not directly measured and not very accurate. For a detailed calculation one would need more reliable density values.

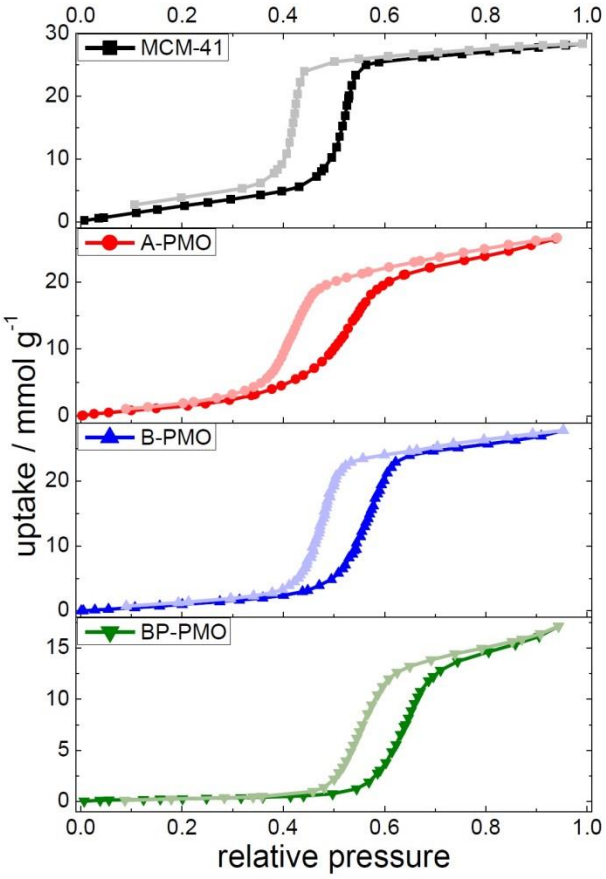

Figure 3S. Water vapor sorption isotherms at 298 K of MCM-41 silica and PMOs.

5. Scanning Electron Microscopy images of the material studied

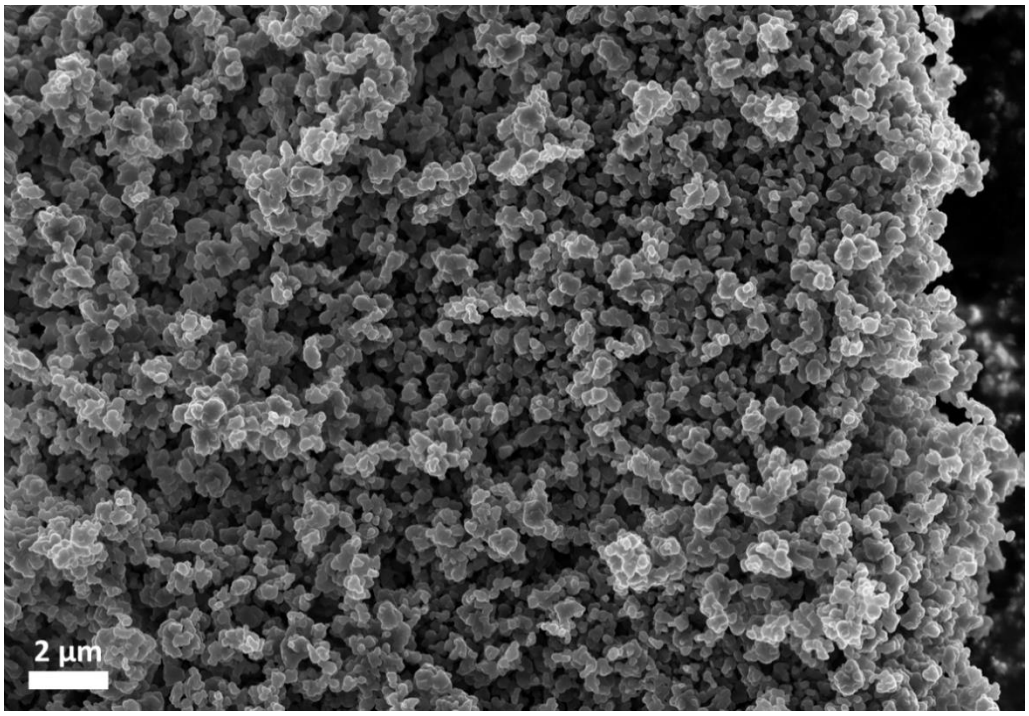

Figure S4. Representative SEM image of MCM-41 silica sample.

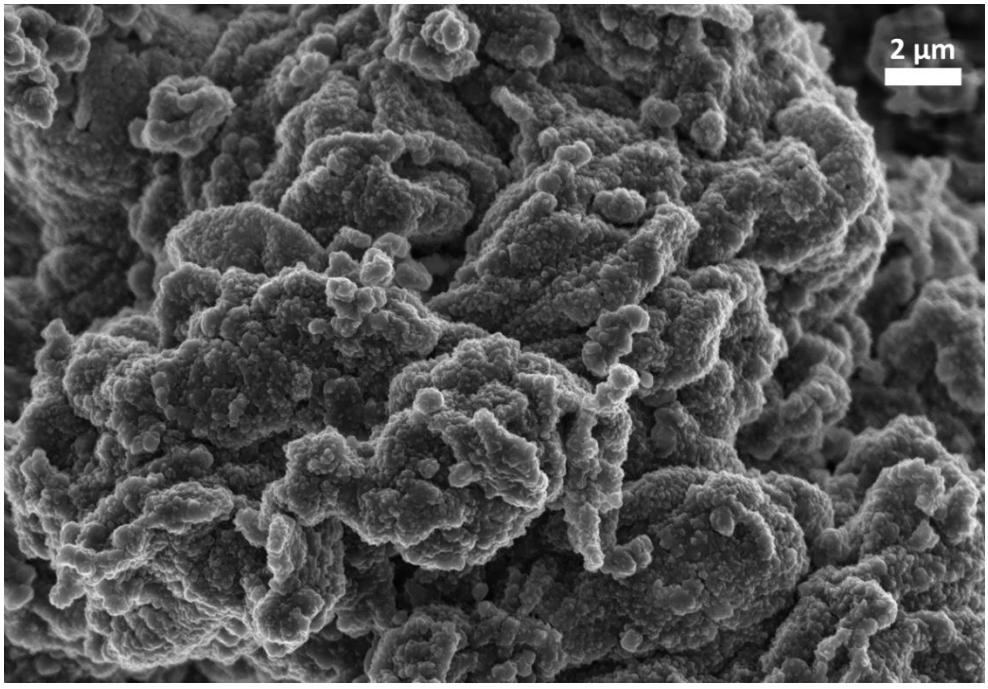

Figure S5. Representative SEM images of A-PMO sample.

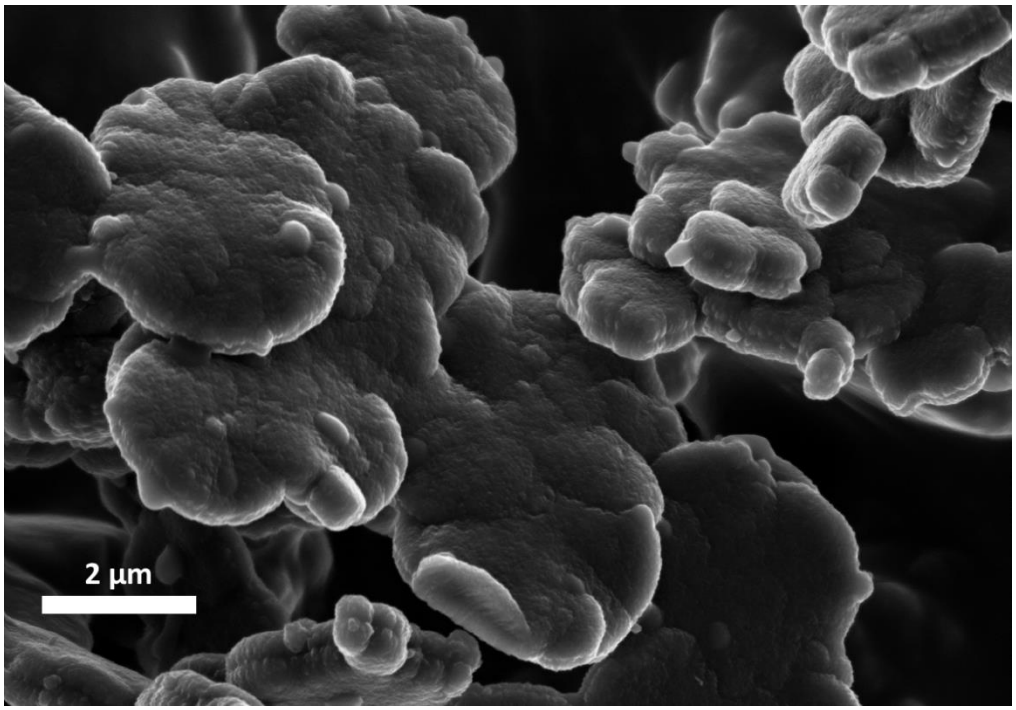

Figure S6. Representative SEM image of B-PMO sample.

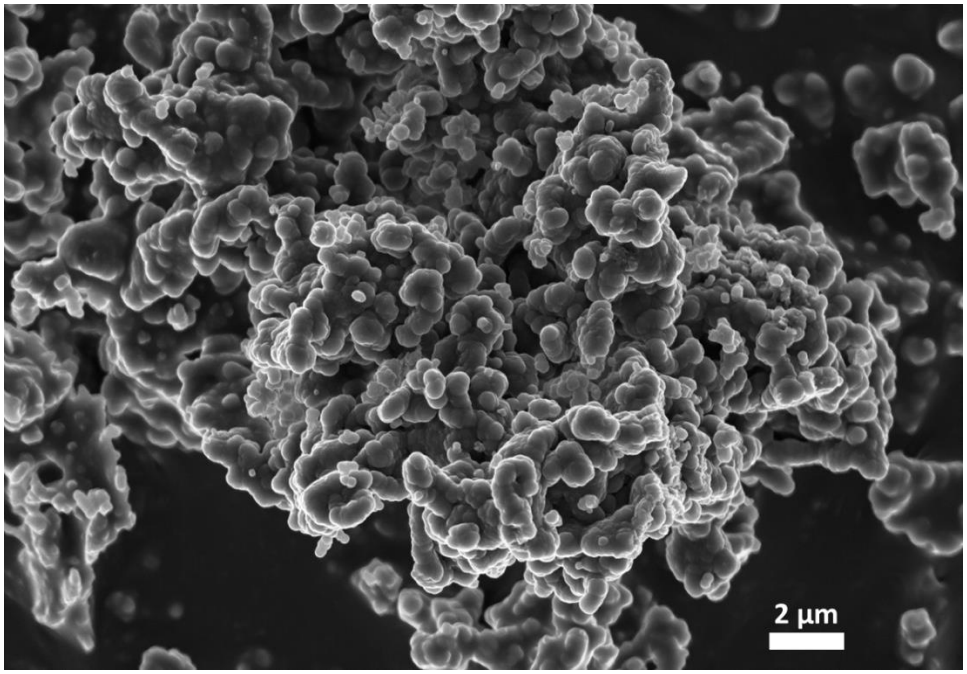

Figure S7. Representative SEM image of BP-PMO sample.

5. Water-saturated sample properties

The two sets of samples have been used for the measurements. The first set was composed of 4 samples of Table 2, which were saturated by water by equilibrating them with a water vapor at 80% humidity. In this way, it has been ensured that all mesopores were completely filled with water and only tiny amount of excess water was found between the particles. The amount of materials and also amount of water after the sample preparation are shown in Table S3.

Table S3. Water saturations in the samples used and estimates of the Knudsen diffusivities and relative fractions of water molecules in the vapor phase..

Sample	Dry material weight (mg)	Weight of adsorbed water (mg)	Water amount per mg of material	Estimate of p_v at 0°C	Estimate of D_v at 0°C	The term p_vD_v
MCM-41	25.08	10.77	0.43	5.5×10^{-6}	1.2×10^{-4}	6.6×10^{-10}
A-PMO	23.28	7.8	0.36	5.9×10^{-6}	1.2×10^{-4}	7.1×10^{-10}
B-PMO	21.59	9.15	0.42	5.3×10^{-6}	1.2×10^{-4}	6.3×10^{-10}
BP-PMO	34.85	5.86	0.17	14.0×10^{-6}	1.2×10^{-4}	16.8×10^{-10}

6. Estimate of the p_vD_v term

An order-of-magnitude estimate of the p_vD_v term can be made as follows. The fraction p_v of water molecules in the vapor phase is defined as $p_v \approx \frac{\rho_v V_v}{m_l}$. V_l is the volume occupied by liquid water and, taking account of the sample preparation which has been done by equilibrating the material with water vapor at 80% humidity, it is reasonable to assume that V_l is equal to the mesopore volume. The volume occupied by the water vapor, which can undergo fast exchange with liquid water in the mesopores, is that formed between particles and particle agglomerates. As an estimate for this quantity, the porosity of a random sphere packing of 0.36 may be used.

V_v is then found as $V_v = 0.36\left(V_p + 1/\rho_{solid}\right)$, where all quantities refer to one gram of material. The p_v values found in this way at T=0°C are shown in Table S3.

For estimating the diffusivities of water molecules in the gas phase, the molecular diffusion regime has been considered. Indeed, the mean free paths of water molecules in gas phase under the conditions of our experiments are of the order of parts of micrometers, i.e. below the void sizes formed between the particles and their agglomerates. Hence, the intermolecular collisions rather than collisions with the particle walls will occur more frequently and thus determine the diffusivities. This diffusivity is as well shown in Table S3.

7. Restricted diffusion in A-PMO sample

Figure S8 shows the time-dependent diffusivities corresponding to the slow diffusing component of the spin-echo diffusion attenuation functions shown in Figure 3 of the main text. This component is associated with the capillary-condensed water in the sample. The diffusion process reflects, thus, water transport along the capillary-condensed phase formed in the A-PMO channels and a continuous liquid film on top of the A-PMO crystals and between them. Decreasing diffusivity with increasing diffusion time *t* is a general feature of restricted diffusion or of fractal character of the space where diffusion takes place. Because the diffusivities measured nicely follow a functional dependency

$$D \propto 1 - \text{const} \times \sqrt{t}$$

we favor the first scenario and anticipate that the experimental observation signals about the short-time regime of restricted diffusion. In this regime

$$D = D_0\left(1 - \frac{4}{9}\frac{S}{V}\sqrt{\frac{D_0 t}{\pi}}\right)$$

where D_0 is bulk diffusivity and S/V is the surface-to-volume ratio of the regions where the molecules diffuse. The analysis using this equation yields diameter of such enclosed domains of about 4 micrometers, which might be associated with an effective agglomerate size in agreement with the data of Figure S5.

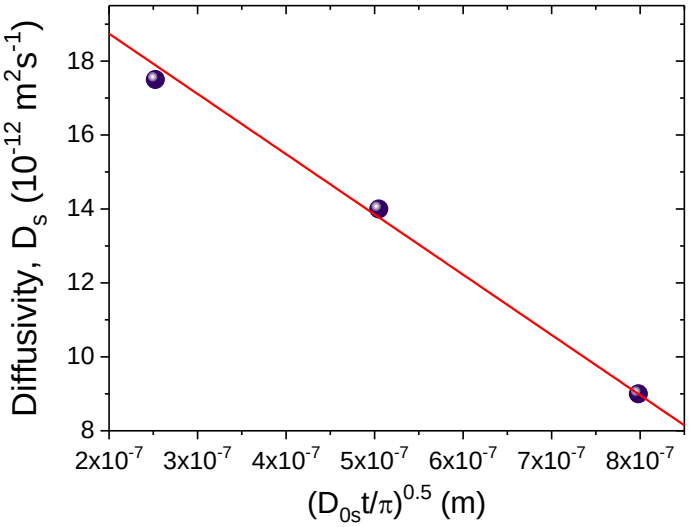

Figure S8. Diffusivities of the capillary-condensed water in the A-PMO sample saturated with water at 80% relative humidity as function measured at different diffusion times from 10 ms to 160 ms. The measurements were performed at T=25°C.

References

[1] F. J. Brieler, M. Fröba, L. Chen, P. J. Klar, W. Heimbrodt, N.-A. Von, A. Loidl, *Chem. Eur. J.* **2002**, *8*, 185–194.

[2] K. Shea, D. Loy, O. Webster, *J. Am. Chem. Soc.* **1992**, *114*, 6700–6710.

[3] S. Martens, R. Ortmann, F. J. Brieler, C. Pasel, Y. J. Lee, D. Bathen, M. Fröba, *Z. Anorg. Allg. Chem.* **2014**, *640*, 632–640.

[4] S. Inagaki, S. Guan, T. Ohsuna, O. Terasaki, *Nature* **2002**, *416*, 304–307.

[5] M. P. Kapoor, Q. Yang, S. Inagaki, *J. Am. Chem. Soc.* **2002**, *124*, 15176–15177.